Bimolecular-reaction effect on the rate constant of electron transfer at the oil/water interface as studied by scanning electrochemical microscopy

Osakai, Toshiyuki
Okamoto, Masanori
Sugihara, Takayasu
Nakatani, Kiyoharu

Bimolecular-reaction effect on the rate constant of electron transfer at the oil/water interface as studied by scanning electrochemical microscopy

Toshiyuki Osakai [a,*], Masanori Okamoto [a], Takayasu Sugihara [b], Kiyoharu Nakatani [c]

[a] *Department of Chemistry, Graduate School of Science, Kobe University, Nada, Kobe 657-8501, Japan*

[b] *Analysis Technology Research Center, Sumitomo Electric Industries Ltd., 1-1-3 Shimaya, Konohana-ku, Osaka 554-0024, Japan*

[c] *Department of Chemistry, Graduate School of Pure and Applied Sciences, University of Tsukuba, 1-1-1 Tennoudai, Tsukuba 305-8571, Japan*

Abstract

Two interfacial electron transfer (ET) systems, *i.e.*, the decamethylferrocene (DcMFc)–$Fe(CN)_6^{3-}$ system and the $MTPP^+$–$Fe(CN)_6^{4-}$ system (M = Zn or Cd; TPP = 5,10,15,20-tetraphenylporphyrin) at oil/water interfaces were studied by means of scanning electrochemical microscopy. The second-order rate constants (k) for the ET systems could be accurately determined at different "standard" Gibbs energies ($\Delta G°$) by changing the nature and concentration ratio of a common ion added to both phases. The driving force dependence, *i.e.*, the log k *vs.* $\Delta G°$ plot did not show a simple upward parabola, with the k values being limited in a certain range of $\Delta G°$. This clearly suggested that there should be a bimolecular -reaction effect, as predicted previously [T. Osakai, H. Hotta, T. Sugihara, K. Nakatani, J. Electroanal. Chem. 571 (2004) 201–206]. However, the observed diffusion-controlled rate constants are typically one-order smaller than the theoretical ones, and have shown only small dependence

on the viscosity of organic solvents for the DcMFc–$Fe(CN)_6^{3-}$ system. These results were unexpected from the previous model based on "microscopic diffusion" of a redox species in the vicinity of the interface, and then suggested an alternative model, in which the rate-determining step is "interfacial diffusion" of a redox species across the oil/water interface.

Keywords: Electron transfer; ITIES; SECM; Bimolecular-reaction effect; Driving force dependence; Marcus theory

---

* Corresponding author. Tel./fax: +81 78 803 5682
E-mail address: osakai@kobe-u.ac.jp (T. Osakai)

1. Introduction

The study of electron transfer (ET) at the interface between two immiscible electrolyte solutions (ITIES) or the so-called oil/water (O/W) interface is useful for understanding not only catalytic reactions in two phase systems (liquid membranes, microemulsions, micelles, *etc.*) but also biological processes occurring at lipid membranes (*e.g.*, respiratory chain, photosynthesis, and antioxidative activity) [1,2]. Since Samec *et al.* [3] reported the first example of an ET reaction at a polarized O/W interface, a variety of interfacial ET systems have been studied by means of electrochemical techniques, which include cyclic voltammetry (CV) [3–8], *ac* impedance method [8,9], current scan polarography [10], CV with micro O/W interfaces [11], scanning electrochemical microscopy (SECM) [12–24], and electrolysis with a single micro O- or W-droplet [25–28]. These experimental studies have shown that reaction mechanisms of ET at O/W interfaces are classified into two categories, *i.e.*, the ion-transfer (IT) mechanism and the ET mechanism [2]. The former involves an IT process of the ionic product of a homogeneous ET in one phase (ordinarily, the W phase). The ferrocene (O)–hexacyanoferrate (W) system, as the first example of a "heterogeneous" ET [3], has been found to come into the IT-mechanism class. The ET mechanism, *i.e.*, a "true" ET reaction can be realized by using a sufficiently hydrophobic redox species in the O phase, *e.g.*, metal complexes of biphthalocyanine [4,5] and 5,10,15,20-tetraphenylporphyrin (TPP) [8].

In the early 1990s, Marcus presented a general theory of ET rates across O/W interfaces [29–33]. An expression was given for the second-order ET rate constant (k). When one can neglect the so-called "work terms", k is given approximately by

$$\ln k = \ln Z - \frac{\lambda\left(1 + \Delta G^{\circ}/\lambda\right)^2}{4RT} \tag{1}$$

where Z is the frequency factor; λ is the reorganization energy; ΔG° is the "standard" Gibbs energy defined by Eq. (8) shown below; R and T have their usual meanings. Before and after the Marcus's study, similar but somewhat different theoretical studies were undertaken by other researchers [34–38]. A parabolic dependence of log k on ΔG°, as predicted from Eq. (1), was

first claimed by Bard and coworkers, who used SECM to determine the k values for the ET reactions between the oxidized zinc complex of TPP ($ZnTPP^+$) and various aqueous reductants [16,19]. However, the experimental log k *vs.* $\Delta G°$ plot showed considerable scatter from the theoretical curve, probably because of the use of the reductants having different intramolecular reorganization energies.

More recently, our group [39] pointed out that an ET reaction at the O/W interface is a bimolecular reaction, so that the "microscopic" diffusion of a redox species in the immediate vicinity of the O/W interface should be not a linear one, but like a hemispherical diffusion. Therefore, we predicted that the k value obtained from kinetic measurements would involve such a bimolecular-reaction effect, having a certain upper limit determined by the microscopic diffusion process. In the previous paper [39], the diffusion-controlled rate constant (k_D) of ET at an O/W interface was formulated in the analogy of the Smoluchowski–Debye theory [40,41] for a bimolecular reaction in a homogeneous medium. If the rate-determining step is the microscopic diffusion of a redox species in the O phase (as expected in ordinary cases), then k_D is given by [42]

$$k_D = 4\pi r_A r_B D_A N \tag{2}$$

where r_A and r_B are the radii of redox species, A and B, added to the O and W phases, respectively; D_A is the diffusion coefficient of A in O; N is Avogadro's number. It is here assumed that species A reacts with species B just when it reaches the "reaction surface" that is shown by shadow in Fig. 1. We then predicted that if the ET process is very fast, the overall or observed rate constant should be restricted by the diffusion-controlled rate constant. This prediction was not inconsistent with the previous kinetic data [19], however no decisive conclusion could be reached because of the scatter of experimental data points. We would like to add that Senda [43] also reported a theory of the bimolecular-reaction effect using a cylindrical-diffusion model.

For verification of our proposed theory [39], we employed CV with a single micro W-droplet to determine the k value for ET between decamethylferrocene (DcMFc) in 2-nitrophenyl octyl ether (NPOE) and $Fe(CN)_6^{3-}$ in the W droplet [27]. In this measurement,

$\Delta G°$ was varied by changing not the aqueous metal complex but the common ion, which was added to both phases to control the Galvani potential difference ($\Delta_O^W\phi \equiv \phi^W - \phi^O$) between the O/W interface. As expected, an upper limit of k was confirmed when $\Delta G°$ was decreased, however further experimental verification was needed.

In this paper, we have employed SECM to perform accurate determination of k for two ET systems, *i.e.*, the $MTPP^+$ (M = Zn, Cd)–$Fe(CN)_6^{4-}$ system and the DcMFc–$Fe(CN)_6^{3-}$ system. In the later system, several organic solvents were used, including 1,2-dichloroethene (DCE), 1,6-dichlorohexane (DCH), nitrobenzene (NB), and NPOE. In these measurements, $\Delta G°$ was varied by changing the nature and concentration ratio of a common ion added to both phases. Based on the log k *vs.* $\Delta G°$ plots prepared for various ET systems, the validity of our theory has been examined comprehensively.

2. Experimental

2.1. Reagents

CdTPP was prepared as reported previously [44] and purified by triple recrystallization from acetone. ZnTPP, DcMFc, and potassium hexacyanoferrate(II) ($K_4Fe(CN)_6$) were purchased from Wako Pure Chemical Industries and used as received.

Tetraphenylborate salts of tetraethyl-, tetrapropyl-, tetrabutyl-, and tetrapentylammonium (TAATPB with TAA = TEA, TPrA, TBA, TPnA) were prepared by metathesis of the corresponding chlorides (all available from Tokyo Chemical Industry) in ethanol with sodium tetraphenylborate (Dojindo Laboratories) in methanol; the resultant crude salts were washed five times with deionized water, followed by recrystallization from acetone–ethanol (1:1). In a similar manner, perchlorate salts of tetrabutyl- and tetrapentylammonium ($TBAClO_4$ and $TPnAClO_4$) were prepared with sodium perchlorate (Aldrich), followed by recrystallization.

DCE for HPLC was purchased from Wako and used without further purification. DCH (98%; Aldrich) was purified by a modified previous method [45]. The purchased reagent was shaken in a separatory funnel with conc. sulfuric acid, and the upper DCH layer was then mixed with activated alumina (Wako; 200 mesh for column chromatography), followed by filtration.

This purification process was repeated several times until either the sulfuric-acid layer or the activated alumina were not colored in brown by impurities. The resultant DCH containing some sulfuric acid was shaken successively with deionized water (emulsification occurred), 10 M sodium hydroxide, and deionized water again, and was finally treated with activated alumina. NB (Wako; analytical grade) and NPOE (Dojindo) were treated before use with activated alumina. All other reagents were of the highest grade available and used as received.

2.2. Apparatus and procedures

The SECM measurements were performed with a commercially available system (HV-402E; Hokuto Denko Co.) combined with a potentiostat (HA1010mM1A). A glass-coated platinum ultramicroelectrode (UME; a 10 μm diameter disc electrode with a glass sheath of 100 μm outer diameter) was used as the probe. For further details of the SECM apparatus, see the previous paper [24]. The SECM measurements were performed in an air-conditioned room at 23 ± 2 °C.

Two types of the electrolytic cells used in SECM are schematically shown in Fig. 2. In Cell A for the DcMFc–$Fe(CN)_6^{3-}$ system, the O phase solvent was DCE, DCH, NB, or NPOE. In Cell B for the $MTPP^+$–$Fe(CN)_6^{4-}$ system, the O phase solvent was NB. Since NB is heavier than water, the test O/W interface in the latter system was prepared at the end of a glass tube of 8 mm inner diameter. To ensure the physical stability of the test interface, the inner glass wall, which should be in contact with the O phase, was siliconized in advance with dimethyldichlorosilane vapor. The O and W solutions were deaerated with nitrogen gas prior to the SECM measurements.

In SECM, the steady-state UME current (I^k) was monitored by moving the UME tip toward an O/W interface at 1.0 μm s^{-1}. A touch of the UME tip to the interface was usually detected by a sudden change of the current. Using the thus-estimated distance (d) between the UME tip and the interface, the plot of I^k against d, a so-called "approach curve" was obtained. The simulation of approach curves was made by using a theoretical model reported previously [12,22]. The UME used in this study is suitable for the simulation, being characterized by $RG = r_g/a = 10$ (r_g = the radius of the glass sheath; a = the radius of the electrode disk) [46].

Prior to the SECM measurements, CV measurements were performed for $Fe(CN)_6^{4-}$ and MTPP (M = Zn, Cd), by using Cells A and B (Fig. 2), respectively. For the oxidation of $Fe(CN)_6^{4-}$ in W, a well-defined sigmoidal wave was observed, as reported previously [27]. For ZnTPP (or CdTPP) in NB, two-successive sigmoidal waves (or a single one) was obtained, corresponding to the two-step (or one-step) one-electron oxidation [8,24]. The one-electron oxidation of DcMFc in organic solvents could also be observed using Cell A, in which the UME tip was penetrated into the lower O phase. Based on these measurements, the working-electrode potential in SECM was set at the potential where the limiting current due to the (first) one-electron oxidation was obtained.

In the SECM measurements, the $\Delta_O^W\phi$ of a test O/W interface was varied by changing the nature and concentration ratio of a common ion in both phases. In the presence of the common ion (X), $\Delta_O^W\phi$ should obey the Nernst equation, being expressed approximately by

$$\Delta_O^W\phi = \Delta_O^W\phi_X^\circ + \frac{RT}{zF}\ln\frac{[X]_O}{[X]_W} \quad (3)$$

where $[X]_O$ and $[X]_W$ are the concentrations of X in O and W, respectively; z is the ionic charge of X; F is the Faraday constant; and $\Delta_O^W\phi_X^\circ$ is the standard ion transfer potential of X. The $\Delta_O^W\phi$ values were estimated by using the literature values of $\Delta_O^W\phi_X^\circ$ [45,47–52].

3. Results and discussion

3.1. Determination of rate constants

Fig. 3 shows two sets of approach curves obtained by SECM measurements with Cells A and B. In the approach curves, the UME tip currents are plotted against the distance (d) between the tip and the test O/W interface. The tip currents are normalized by those at long distances where they showed constant values. As shown in Fig. 3, the normalized currents at shorter distances increased markedly with the concentrations of DcMFc and $Fe(CN)_6^{4-}$ for Cells A and B, respectively. These results clearly showed that the following redox reactions occurred in the respective cells.

For Cell A:

$Fe(CN)_6^{4-} \rightarrow Fe(CN)_6^{3-} + e^-$ (at the UME in W) (4)

$Fe(CN)_6^{3-}(W) + DcMFc(O) \rightarrow Fe(CN)_6^{4-}(W) + DcMFc^+(O)$ (at the O/W interface) (5)

For Cell B (with M = Zn, Cd):

$MTPP \rightarrow MTPP^+ + e^-$ (at the UME in O) (6)

$MTPP^+(O) + Fe(CN)_6^{4-}(W) \rightarrow MTPP(O) + Fe(CN)_6^{3-}(W)$ (at the O/W interface) (7)

In both the systems, experimental approach curves fit well with the theoretical curves, as shown in Fig. 3, although the experimental blank curves tended to deviate slightly upward from the theoretical ones (a possible origin for the deviation may be impurities). Then, the apparent first-order rate constants (k_f) were successfully obtained as the fitting parameter for different concentrations of the redox species. Because k_f is related to the second-order rate constant (k) as $k_f = k$[DcMFc] (Cell A) or $k_f = k[Fe(CN)_6^{4-}]$ (Cell B), the k_f value should be proportional to [DcMFc] or $[Fe(CN)_6^{4-}]$. In practice, a good proportionality was observed in a definite concentration range under most conditions studied (Fig. 4). From the slope of the linear plot, the k value could thus be accurately determined. The relative SD (=standard deviation) for k was typically within 10%.

Tables 1 and 2 show the kinetic data for the NB/W interface, which were obtained with Cells A and B, respectively, under different electrolyte conditions, *i.e.*, at different $\Delta_O^W\phi$ values. As seen in Table 2, the kinetic data for CdTPP could be obtained only under a single electrolyte condition, probably owing to the relative instability of CdTPP. Similar kinetic data obtained with Cell A for other O/W interfaces are presented in Tables S1–S3 (Supplementary information).

3.2. Driving force dependence of the rate constants

The dependence of the ET rate constant on the driving force ($\Delta G°$) was investigated. The value of $\Delta G°$ is given by

$$-\Delta G° = \pm F(E_W^{o'} - E_O^{o'} + \Delta_O^W\phi) \quad (8)$$

where $E_W^{\circ'}$ and $E_O^{\circ'}$ are the formal potentials of the redox couples in W and O, respectively, being expressed on the same potential scale; the positive and negative signs of the right-hand side of Eq. (8) correspond to Cells A and B, respectively; note that $\Delta G°$ is defined as the "standard" Gibbs energy of the forward (left-to-right) reaction of Eqs. (5) and (7). In the present SECM measurements, $\Delta G°$ could be evaluated from the difference of the formal potentials measured by positioning the UME tip in W and O, which equals to ($E_W^{\circ'} - E_O^{\circ'} + \Delta_O^W\phi$) in the right-hand side of Eq. (8).

Fig. 5 shows the $\Delta G°$ dependence of k for the ET between DcMFc in NB and $Fe(CN)_6^{3-}$ in W. The log k *vs.* $\Delta G°$ plot did not show a simple upward parabola, with the k value being limited in the lower $\Delta G°$ range, as previously reported for the NPOE/W interface [27]. In this study, a similar dependence was observed for the DCE/W, DCH/W, and NPOE/W interfaces (Figs. S1–S3, Supplementary material). These results clearly suggest that there should be a rate-limiting process for the ET reactions, which is hardly affected by the interfacial potential. The limiting process might be the previously proposed "microscopic" diffusion of a redox species in O or W, prior to the succeeding ET reaction at the O/W interface [39]. We have then assumed the following reaction scheme:

$$\mathrm{A(O)} + \mathrm{B(W)} \underset{k_{uni}}{\overset{\text{diffusion } k_D}{\rightleftharpoons}} \mathrm{A\cdots B} \xrightarrow{\text{ET } k_{ET}} \text{products} \tag{9}$$

where A···B represents the encounter complex of A and B; k_{uni} is the dissociation rate constant of A···B; k_{ET} is the first-order heterogeneous rate constant of the intramolecular ET. The overall second-order rate constant, *i.e.*, k is then given by

$$k = \frac{k_D k_{ET}}{k_{ET} + k_{uni}} \tag{10}$$

With a treatment similar to that for a homogeneous reaction in solution [53,54], k_{uni} (cm s^{-1}) can be estimated from k_D (cm M^{-1} s^{-1}) as

$$k_{uni} = \left(\frac{10^{-3}}{N}\right)\frac{k_D}{\Delta V} \tag{11}$$

where the volume ΔV (cm^3) contains the encounter complex and is given approximately by $(4/3)\pi(r_A+r_B)^3$. For the estimation of ΔV and thus k_{uni}, the following values were used for r_A or r_B: 0.48 nm (DcMFc [55,56]), 0.62 nm ($MTPP^+$ [8]), 0.44 nm ($Fe(CN)_6^{3-}$ [55]), and 0.45 nm ($Fe(CN)_6^{4-}$ [57]).

Regarding k_{ET}, an Arrhenius-type general kinetic equation was assumed:

$$k_{ET} = \kappa Z_{het} \exp\left(-\frac{\Delta G^{\ddagger}}{RT}\right) \tag{12}$$

where κ is the Landau–Zener non-adiabacity factor ($\kappa = 1$ for an adiabatic reaction); Z_{het} is the frequency factor; $\Delta G^{\ddagger}$ is the Gibbs energy of activation of the reaction, which may be estimated using the theoretical equation by Marcus [29–33].

$$\Delta G^{\ddagger} = w^{r} + \frac{\lambda}{4}\left(1 + \frac{\Delta G^{\circ} + w^{p} - w^{r}}{\lambda}\right)^2 \tag{13}$$

where w^r and w^p are the work terms, respectively, for bringing the reactants from infinite distance and for removing the products to the infinite distance. These work terms, however, are usually much lower than λ, as shown previously [8]. Accordingly, $\Delta G^{\ddagger}$ can be approximated by

$$\Delta G^{\ddagger} = \frac{\lambda}{4}\left(1 + \frac{\Delta G^{\circ}}{\lambda}\right)^2 \tag{14}$$

Using Eqs. (10)–(12), and (14), manual curve fitting was performed for the log *k vs.* ΔG° plot in Fig. 5. When k_D, κZ_{het}, and λ were used as adjusting parameters, however, curve fitting was successful for various sets of κZ_{het}, and λ. We therefore estimated the λ value theoretically, as described below, to reduce the adjusting parameters to two, *i.e.*, k_D and κZ_{het}. As shown by the solid line in Fig. 5, the theoretical curve was well fitted to the experimental data. Such curve fitting was also successful for the log *k vs.* ΔG° plots (Figs. S1–S3, Supplementary information). Table 3 shows the values of k_D and κZ_{het} obtained as the adjusting parameters and the theoretically estimated values of λ.

The reorganization energy was estimated as follows: λ is defined by $\lambda = \lambda_{out} + \lambda_{in}$, where λ_{out} and λ_{in} are the outer- and inner-sphere reorganization energies, respectively. Marcus [29,30] gave the equation for λ_{out}:

$$\lambda_{\mathrm{out}} = \frac{N(ne)^2}{4\pi\varepsilon_0}\left[\frac{1}{2r_{\mathrm{A}}}\left(\frac{1}{\varepsilon_{\mathrm{O}}^{\mathrm{op}}}-\frac{1}{\varepsilon_{\mathrm{O}}^{\mathrm{s}}}\right)+\frac{1}{2r_{\mathrm{B}}}\left(\frac{1}{\varepsilon_{\mathrm{W}}^{\mathrm{op}}}-\frac{1}{\varepsilon_{\mathrm{W}}^{\mathrm{s}}}\right)\right.$$
$$-\frac{1}{4d_1}\left(\frac{\varepsilon_{\mathrm{W}}^{\mathrm{op}}-\varepsilon_{\mathrm{O}}^{\mathrm{op}}}{\varepsilon_{\mathrm{O}}^{\mathrm{op}}(\varepsilon_{\mathrm{W}}^{\mathrm{op}}+\varepsilon_{\mathrm{O}}^{\mathrm{op}})}-\frac{\varepsilon_{\mathrm{W}}^{\mathrm{s}}-\varepsilon_{\mathrm{O}}^{\mathrm{s}}}{\varepsilon_{\mathrm{O}}^{\mathrm{s}}(\varepsilon_{\mathrm{W}}^{\mathrm{s}}+\varepsilon_{\mathrm{O}}^{\mathrm{s}})}\right)$$
$$-\frac{1}{4d_2}\left(\frac{\varepsilon_{\mathrm{O}}^{\mathrm{op}}-\varepsilon_{\mathrm{W}}^{\mathrm{op}}}{\varepsilon_{\mathrm{W}}^{\mathrm{op}}(\varepsilon_{\mathrm{O}}^{\mathrm{op}}+\varepsilon_{\mathrm{W}}^{\mathrm{op}})}-\frac{\varepsilon_{\mathrm{O}}^{\mathrm{s}}-\varepsilon_{\mathrm{W}}^{\mathrm{s}}}{\varepsilon_{\mathrm{W}}^{\mathrm{s}}(\varepsilon_{\mathrm{O}}^{\mathrm{s}}+\varepsilon_{\mathrm{W}}^{\mathrm{s}})}\right)$$
$$\left.-\frac{2}{l}\left(\frac{1}{\varepsilon_{\mathrm{O}}^{\mathrm{op}}+\varepsilon_{\mathrm{W}}^{\mathrm{op}}}-\frac{1}{\varepsilon_{\mathrm{O}}^{\mathrm{s}}+\varepsilon_{\mathrm{W}}^{\mathrm{s}}}\right)\right] \quad (15)$$

where n is the number of electrons transferred (here, $n = 1$); ε_0 is the permittivity of vacuum; $\varepsilon_i^{\mathrm{s}}$ and $\varepsilon_i^{\mathrm{op}}$ are the static and optical dielectric constants of solvent i (=O and W); d_i is the distance from the interface to the center of the reactant or product in solvent i; and l is the distance between the centers of the reactants. In the present estimation, we simply assumed that $d_1 = r_{\mathrm{A}}$, $d_2 = r_{\mathrm{B}}$, and $l = r_{\mathrm{A}} + r_{\mathrm{B}}$. The dielectric constants used are: $\varepsilon_i^{\mathrm{s}} = 35.0$ (NB [58]), 10.4 (DCE [58]), 8.83 (DCH [45]), 24.2 (NPOE [52]), 78.8 (W [58]); $\varepsilon_i^{\mathrm{op}} = 2.4$ (NB [58]), 2.0 (DCE [58]), 2.12 (DCH [59]), 2.3 (NPOE [60]), 1.8 (W [58]). Then, we evaluated the outer-sphere contribution to the reorganization energy as $\lambda_{\mathrm{out}} = 71.1$, 72.2, 68.9, and 71.5 kJ mol^{-1} for the NB/W, DCE/W, DCH/W, and NPOE/W interfaces, respectively. The inner-sphere contributions from $Fe(CN)_6^{3-}$ and DcMFc are reported as $\lambda_{\mathrm{in}}(Fe(CN)_6^{3-}) = 10.6$ kJ mol^{-1} (=0.11 eV [61]) and $\lambda_{\mathrm{in}}(\mathrm{DcMFc}) =$ 0.6 kJ mol^{-1} (= 0.15 kcal mol^{-1} [62]), therefore $\lambda_{\mathrm{in}} = \lambda_{\mathrm{in}}(Fe(CN)_6^{3-}) + \lambda_{\mathrm{in}}(\mathrm{DcMFc}) = 11.2$ kJ mol^{-1}. Finally, the values of λ ($\approx \lambda_{\mathrm{out}} + \lambda_{\mathrm{in}}$) could be estimated as shown in Table 3.

Fig. 6 shows the driving force dependence of k for the ET between $MTPP^+$ (M = Zn, Cd) in NB and $Fe(CN)_6^{4-}$ in W. The plot for $CdTPP^+$ (△) is based on the data previously obtained by *ac* impedance method [8]. By including this plot, curve fitting was successfully performed to obtain the theoretical curve as shown by the solid line in Fig. 6. In this curve fitting, λ was also used as an adjusting parameter. The obtained values of k_{D}, κZ_{het}, and λ are shown in Table 3. The value of λ (=43 kJ mol^{-1}) is somewhat smaller than the theoretically estimated value of 77.0 kJ mol^{-1} [8] and the literature value of 82 kJ mol^{-1} (=0.85 eV [19]); this literature value was obtained by SECM, but with various aqueous reductants and some different organic solvents. The present SECM measurements were performed at a single O/W interface by using

the sole aqueous reductant ($Fe(CN)_6^{4-}$). Although two different organic oxidants (*i.e.*, tip-generated $ZnTPP^+$ and $CdTPP^+$) were used here, the inner-sphere reorganization energy of such large complexes seems to be negligible. In Fig. 6, another fitting curve is shown by the dashed line, which was obtained with the theoretical value of k_D (=40 cm M^{-1} s^{-1}; estimated from Eq. (2)) and the adjusting parameters of κZ_{het} and λ. As seen in the figure, however, a less satisfactory fitting result was obtained.

Due to the proper arrangement of experimental conditions, we could thus obtain the clear driving-force dependence shown in Fig. 6. The dependence is apparently different from the parabolic one that was claimed by Bard and coworkers [16,19]. There seems to be an upper limit of k, which seems to be due to a bimolecular-reaction effect. According to the previous reports [16,19], however, the existence of a Marcus inverted region was confirmed in this study as well.

Here, it is interesting to compare the experimental values of κZ_{het} with those predicted using the Marcus theory. The second-order rate constant, k, under ET-controlled conditions (*i.e.*, $k_{ET} << k_{uni}$), is related to the first-order rate constant, k_{ET}, as $k = Kk_{ET} = (k_D/k_{uni})k_{ET}$ [2,39]. Since k and k_{ET} are given by $k = Z\exp(-\Delta G^{\ddagger}/RT)$ and Eq. (12), respectively, we obtain a relation: $Z = (k_D/k_{uni})\kappa Z_{het}$. Using the experimental values of κZ_{het}, k_D, and k_{uni} (see Table 3), Z can be calculated, *e.g.*, as Z = 12 cm M^{-1} s^{-1} for the $MTPP^+$–$Fe(CN)_6^{4-}$ system. On the other hand, Marcus [29–33] proposed that the frequency factor Z for a "sharp" O/W interface is given by

$$Z = 2\pi(r_A + r_B)\kappa\nu(\Delta l)^3 \quad (16)$$

where κ is the transmission coefficient (κ = 1 for a perfect adiabatic ET), ν is the frequency for molecular motion, and Δl is the parameter appearing in an exponent for the dependence of the ET rate [$\propto\exp(-l/\Delta l)$] on separation distance l. Using the typical values, $\kappa\nu = 10^{12}$ s^{-1} and Δl = 0.1 nm, adopted by Marcus [32], the Z value is estimated to be 410 cm M^{-1} s^{-1} for the $MTPP^+$–$Fe(CN)_6^{4-}$ system. This value is one-order higher than the above experimental value (*i.e.*, 12 cm M^{-1} s^{-1}). In a similar manner, the Z value for the DcMFc–$Fe(CN)_6^{3-}$ system is estimated to be 350 cm M^{-1} s^{-1}. In this case, the theoretical value of Z is rather lower than the experimental values, Z = 670, 1700, 3700, 4200 cm M^{-1} s^{-1} for the DCE/W, NB/W, DCH/W,

and NPOE/W interfaces, respectively. Thus, though the reason is not clear yet, it has been found that the observed frequency factor is largely dependent not only on the nature of redox species in the O phase but also on the nature of the organic solvent.

3.3. Effects of organic solvents

According to Eq. (2), k_D should be proportional to D_A, *i.e.*, the diffusion coefficient of A (= DcMFc) in the O phase. Since D_A is inversely proportional to the viscosity (η) of the solvent, k_D should be linearly dependent on η^{-1}. As seen in Table 3, the obtained values of k_D were decreased with the order of η, *i.e.*, DCE < NB < DCH < NPOE. However, it should be noted that k_D was not simply proportional to η^{-1}; the dependence was considerably less than that expected from Eq. (2). Also, as discussed below, the k_D values are considerably smaller than the theoretical ones (see also Table 3).

In our previous study with a single micro W-droplet [27], a similar log k *vs.* $\Delta G°$ plot to that obtained in this study was observed for the ET between DcMFc in NPOE and $Fe(CN)_6^{3-}$ in W. As shown in Fig. S3 (Supplementary information), however, the previous k values at lower $\Delta G°$ values are about four times larger than those determined by SECM. Considering the possible experimental errors in kinetic measurements, the discrepancy between the two data sets may not be very significant. Possible origins of the discrepancy are the nonideality of the electrode configuration in SECM (*e.g.*, inclination of the UME axis with respect to the normal to the O/W interface) and the imperfection of the cylinder model employed for the digital simulation in CV with a micro W-droplet.

3.4. Alternative model

As described above, the k_D values obtained in SECM showed only a small dependence on the organic-solvent viscosity. Also, the k_D values are typically one-order smaller than those estimated from Eq. (2). Such unexpected results might suggest the invalidity of the previous model for a diffusion-controlled bimolecular reaction [39].

Then we propose an alternative model for understanding the bimolecular-reaction effect. Fig. 7b shows the new model, which is based on the "interfacial diffusion" of redox species across the O/W interface. It is here assumed that the rate-determining step is the interfacial

diffusion of species B in W toward species A in O. If species A is not surface active and thus does not exist on the O/W interface, then species B should cross the inner layer of the interface to react with species A. In the inner layer, the water molecules contacting with the organic solvents probably form a planer hydrogen-bonded network, which is similar to the structure making of water molecules hydrated to a strongly hydrophobic ion such as TBA^+. Accordingly, there would be a certain energy barrier for the redox species to break the hydrogen-bonded network. Such a transport process across the inner layer, which we here call "interfacial diffusion", may be a rate-determining step of the overall ET reaction, although some molecular dynamic simulation [63] showed that there is no significant slowing down as a semi-hydrophobic tetramethylammonium ion crosses an O/W interface. For species B being fully hydrophilic and having a large positive free energy of transfer, however, the interfacial diffusion would show an appreciably large activation energy. It is then considered that the diffusion rate would be influenced by rheological properties of the O/W interface rather than those of the bulk phase (*e.g.*, viscosity of the organic solvent). As previously discussed on ion-transfer kinetics at an O/W interface [64], the interfacial tension (γ) should significantly influence the transfer kinetics of redox species across the O/W interface. Regarding the interfaces studied here, however, the γ values show no large differences: γ (in mN m^{-1}) = 28.4 (DCE/W [65]), 25.2 (NB/W [66]), 23.5 (DCH/W [67]), 27.9 (NPOE/W [68]). This might have resulted in the small dependence of k_D on the nature of organic solvents. It should also be pointed out that the postulated interfacial diffusion process for charged redox species (*e.g.*, $Fe(CN)_6^{3-}$) should be affected by the inner layer potential difference. However, this effect seems to be restricted, because the inner layer potential difference of an O/W interface is generally small compared with the potential difference across the diffuse layers in O and W [69,70].

Thus, the present kinetic data obtained by SECM have suggested the new model based on "interfacial diffusion" (Fig. 7b). Nevertheless, the previous model based on "microscopic diffusion" (Fig. 7a) cannot be entirely excluded, since the CV measurements with a micro W-droplet have given higher rate constants closer to the theoretical values of k_D. Further

detailed studies would be required to clarify this issue.

4. Conclusions

Regarding the two ET systems, *i.e.*, the $MTPP^+$ (M = Zn, Cd)–$Fe(CN)_6^{4-}$ system and the DcMFc–$Fe(CN)_6^{3-}$ system, the following conclusions have been reached.

1) The second-order rate constants (k) for the two ET systems could be accurately determined by means of SECM.
2) For both ET systems, the driving force dependence of the rate constant, *i.e.*, the log k *vs.* $\Delta G°$ plots did not show a simple upward parabola, with the k values being limited in a certain range of $\Delta G°$. This suggests that the ET rates should be limited by the "microscopic" diffusion of redox species, as predicted in the previous study [39].
3) The diffusion-controlled rate constants obtained experimentally, however, are typically one-order smaller than the theoretical values, and have shown only small dependence on the viscosity of organic solvents. These results suggest an alternative model, in which the rate-determining step is the "interfacial" diffusion of a redox species across the O/W interface.

Acknowledgements

This work was supported by a Grant-in-Aid from the Ministry of Education, Culture, Sports, Science and Technology of Japan (No. 16550073).

Appendix A. Supplementary material

Supplementary data associated with this article can be found, in the online version, doi:10.1016/j.jelechem.2009.01.001.

References and notes

[1] D.J. Fermín, H. Jensen, H.H. Girault, in: A. J. Bard, M. Stratmann, E.J. Calvo (Eds.), Encyclopedia of Electrochemistry, vol. 2: Interfacial Kinetics and Mass Transport, Wiley-VCH, Weinheim, 2003, pp. 360–390.

[2] T. Osakai, H. Hotta, in: H. Watarai, N. Teramae, T. Sawada, (Eds.), Interfacial Nanochemistry, Kluwer Academic/Plenum, New York, 2005 (Chapter 8).

[3] Z. Samec, V. Mareček, J. Weber, J. Electroanal. Chem. 103 (1979) 11–18.

[4] G. Geblewicz, D.J. Schiffrin, J. Electroanal. Chem. 244 (1988) 27–37.

[5] V.J. Cunnane, D.J. Schiffrin, C. Betran, G. Geblewicz, T. Solomon, J. Electroanal. Chem. 247 (1988) 203–214.

[6] Y. Cheng, D.J. Schiffrin, J. Electroanal. Chem. 314 (1991) 153–163.

[7] H. Hotta, S. Ichikawa, T. Sugihara, T. Osakai, J. Phys. Chem. B 107 (2003) 9717–9725.

[8] T. Osakai, S. Ichikawa, H. Hotta, H. Nagatani, Anal. Sci. 20 (2004) 1567–1573.

[9] Y. Cheng, D.J. Schiffrin, J. Chem. Soc. Faraday Trans. 89 (1993) 199–205.

[10] S. Kihara, M. Suzuki, K. Maeda, K. Ogura, M. Matsui, J. Electroanal. Chem. 271 (1989) 107–125.

[11] B. Quinn, R. Lahtinen, L. Murtomäki, K. Kontturi, Electrochim. Acta 44 (1998) 47–57.

[12] C. Wei, A.J. Bard, M.V. Mirkin, J. Phys. Chem. 99 (1995) 16033–16042.

[13] M. Tsionsky, A.J. Bard, V.M. Mirkin, J. Phys. Chem. 100 (1996) 17881–17888.

[14] M. Tsionsky, A.J. Bard, M.V. Mirkin, J. Am. Chem. Soc. 119 (1997) 10785–10792.

[15] B. Liu, M.V. Mirkin, J. Am. Chem. Soc. 121 (1999) 8352–8355.

[16] A.L. Barker, P.R. Unwin, S. Amemiya, J. Zhou, A.J. Bard, J. Phys. Chem. B 103 (1999) 7260–7269.

[17] J. Zhang, A.L. Barker, P.R. Unwin, J. Electroanal. Chem. 483 (2000) 95–107.

[18] S. Amemiya, Z. Ding, J. Zhou, A.J. Bard, J. Electroanal. Chem. 483 (2000) 7–17.

[19] Z. Ding, B.M. Quinn, A.J. Bard, J. Phys. Chem. B 105 (2001) 6367–6374.

[20] Z. Zhang, Y. Yuan, P. Sun, B. Su, J. Guo, Y. Shao, H.H. Girault, J. Phys. Chem. B 106 (2002) 6713–6717.

[21] B. Liu, M.V. Mirkin, J. Phys. Chem. B 106 (2002) 3933–3940.

[22] M.V. Mirkin, M. Tsionsky, in: A.J. Bard, M.V. Mirkin (Eds.), Scanning Electrochemical Microscopy, Marcel Dekker, New York, 2003 (Chapter 8).

[23] X. Lu, M. Nan, H. Zhang, X. Liu, H. Yuan, J. Yang, J. Phys. Chem. C 111 (2007) 14998–15002.

[24] T. Sugihara, T. Kinoshita, S. Aoyagi, Y. Tsujino, T. Osakai, J. Electroanal. Chem. 612 (2008) 241–246.

[25] K. Nakatani, K. Chikama, H.-B. Kim, N. Kitamura, Chem. Phys. Lett. 237 (1995) 133–136.

[26] K. Chikama, K. Nakatani, N. Kitamura, Bull. Chem. Soc. Jpn. 71 (1998) 1065–1070.

[27] K. Nakatani, J. Yamashita, T. Negishi, T. Osakai, J. Electroanal. Chem. 575 (2005) 27–32.

[28] K. Nakatani, M. Uchino, S. Suzuki, T. Negishi, T. Osakai, Anal. Sci. 25 (2009) 25 (2009) 183–187.

[29] R.A. Marcus, J. Phys. Chem. 94 (1990) 1050–1055.

[30] R.A. Marcus, J. Phys. Chem. 94 (1990) 4152–4155.

[31] R.A. Marcus, J. Phys. Chem. 94 (1990) 7742 (corrections).

[32] R.A. Marcus, J. Phys. Chem. 95 (1991) 2010–2013.

[33] R.A. Marcus, J. Phys. Chem. 99 (1995) 5742 (corrections).

[34] Y.I. Kharkats, Sov. Electrochem. 12 (1976) 1257–1263.

[35] H.H. Girault, J. Electroanal. Chem. 388 (1995) 93–100.

[36] A.G. Volkov, D.W. Deamer, Progr. Colloid Polym. Sci. 103 (1997) 21–28.

[37] W. Schmickler, J. Electroanal. Chem. 428 (1997) 123–127.

[38] I. Benjamin, Y.I. Kharkats, Electrochim. Acta 44 (1998) 133–138.

[39] T. Osakai, H. Hotta, T. Sugihara, K. Nakatani, J. Electroanal. Chem. 571 (2004) 201–206.

[40] M.V. Smoluchowski, Z. Phys. Chem. 92 (1917) 129–168.

[41] P. Debye, Trans. Electrochem. Soc. 82 (1942) 265–272.

[42] In the paper [39], the diffusion-controlled rate constant was given by somewhat complicated expressions, however it can be expressed more simply as in Eq. (2).

[43] M. Senda, Rev. Polarogr. 49 (2003) 31–35 (erratum: 49 (2003) 106).

[44] A.D. Adler, F.R. Longo, F. Kampas, J. Kim, J. Inorg. Nucl. Chem. 32 (1970) 2443–2445.

[45] H. Katano, H. Tatsumi, M. Senda, Talanta 63 (2004) 185–193.

[46] M.V. Mirkin, in: A.J. Bard, M.V. Mirkin (Eds.), Scanning Electrochemical Microscopy, Marcel Dekker, New York, 2003 (Chapter 5).

[47] T. Osakai, Rev. Polarogr. 52 (2006) 3–12.

[48] T. Osakai, K. Ebina, J. Phys. Chem. B 102 (1998) 5691–5698; the errata is available from http://www2.kobe-u.ac.jp/~osakai/OldPapers.html.

[49] Z. Samec, D. Homolka, V. Mareček, L. Kavan, J. Electroanal. Chem. 145 (1983) 213–218.

[50] A. Sabela, V. Mareček, Z. Samec, R. Fuoco, Electrochim. Acta 37 (1992) 231–235.

[51] S. Wilke, T. Zerihun, J. Electroanal. Chem. 515 (2001) 52–60.

[52] Z. Samec, J. Langmaier, A. Trojánek, J. Electroanal. Chem. 409 (1996) 1–7.

[53] D. Rehm, A. Weller, Israel J. Chem. 8 (1970) 259–271.

[54] J.I. Steinfeld, J.S. Francisco, W.L. Hase, Chemical Kinetics and Dynamics, Prentice Hall, Englewood Cliffs, NJ, 1989 (Chapter 4).

[55] A. Zahl, R. van Eldik, M. Matsumoto, T.W. Swaddle, Inorg. Chem. 42 (2003) 3718–3722.

[56] M. Matsumoto, T.W. Swaddle, Inorg. Chem. 43 (2004) 2724–2735.

[57] Y. Marcus, Ion Properties, Marcel Dekker, New York, 1997 (Chapter 3).

[58] V.S. Markin, A.G. Volkov, Electrochim. Acta 34 (1989) 93–107.

[59] Estimated as $\varepsilon_i^{\mathrm{op}} = n_{\mathrm{D}}^2$, where n_{D} is the refractive index (= 1.457; D.R. Lide (Ed.), CRC Handbook of Chemistry and Physics, 82nd ed., CRC Press, Boca Raton, FL, 2001).

[60] Estimated from n_{D} (= 1.508; Beilsteins Handbuch der Organischen Chemie, 4th ed., Springer-Verlag, Berlin, 1978, vol. 6, part 3, p. 1251).

[61] P. Delahay, Chem. Phys. Lett. 99 (1983) 87–88.

[62] T. Gennett, D.F. Milner, M.J. Weaver, J. Phys. Chem. 89 (1985) 2787–2794.

[63] K. Schweighofer, I. Benjamin, J. Phys. Chem. A 103 (1999) 10724–10729.

[64] K. Aoki, Electrochim. Acta 41 (1996) 2321–2327.

[65] H.H. Girault, D.J. Schiffrin, B.D.V. Smith, J. Colloid Interface Sci. 101 (1984) 257–266.

[66] D.J. Donahue, F.E. Bartell, J. Phys. Chem. 56 (1952) 480–484.

[67] Determined by the drop-time method (S. Sawada, T. Osakai, M. Senda, Bunseki Kagaku 45 (1996) 1045–1049).

[68] H. Boerrigter, T. Tomasberger, A.S. Booij, W. Verboom, D.N. Reinhoudt, F.J. de Jong, Membr. Sci. 165 (2000) 273–291.

[69] Z. Samec, V. Mareček, D. Homolka, Faraday Discuss. Chem. Soc. 77 (1984) 197–208.

[70] M. Senda, T. Kakiuchi, T. Osakai, T. Kakutani, in: V.E. Kazarinov (Ed.), The Interface Structure and Electrochemical Processes at the Boundary Between Two Immiscible Liquids, Springer-Verlag, Berlin, 1987, pp. 107–121.

Table 1

Kinetic data obtained with Cell A for the NB/W interface

Electrolyte conditions	$\Delta_O^W\phi$ [a] (V)	$\Delta G°$ [b] (kJ mol^{-1})	k_f (cm s^{-1}) [DcMFc] (M) 0.0015	0.003	0.005	0.007	$k \pm$ SD (cm M^{-1} s^{-1})
(I) 50 mM TEATPB (O)–10 mM TEACl (W)	–0.014	–37		0.0135	0.0230	0.0315	4.53 ± 0.06
(II) 20 mM TEATPB (O)–20 mM TEACl (W)	–0.055	–33	0.0060	0.0140	0.0220	0.0310	4.27 ± 0.28
(III) 20 mM TPrATPB (O)–20 mM TPrACl (W)	–0.170	–22		0.0130	0.0220	0.0310	4.39 ± 0.05
(IV) 10 mM TPrATPB (O)–50 mM TPrACl (W)	–0.211	–18		0.0140	0.0230	0.0320	4.61 ± 0.05
(V) 20 mM TBATPB (O)–20 mM TBACl (W)	–0.275	–12		0.0090	0.0140	0.0200	2.89 ± 0.10
(VI) 20 mM TPnATPB (O)–20 mM TPnACl (W)	–0.408	–1		—[c]	0.0016	0.0022	0.32 ± 0.00

[a] Estimated from Eq. (3) with the reported values of $\Delta_O^W\phi_X^\circ$ [47–49].

[b] Calculated by Eq. (8) with $E_W^{\circ'} - E_O^{\circ'} = 0.40$ V.

[c] The value was too small to determine.

Table 2

Kinetic data obtained with Cell B for the NB/W interface

Electrolyte conditions	$\Delta_O^W\phi$ [a] (V)	$\Delta G°$ [b] (kJ mol^{-1})	k_f (cm s^{-1}) [$Fe(CN)_6^{4-}$] (M) 0.001	0.0015	0.002	0.0025	0.004	$k \pm$ SD (cm M^{-1} s^{-1})
ZnTPP								
(I) 0.1 M $TPnAClO_4$ (O)–20 mM TPnACl (W)	–0.367	–82	—[c]	—[c]	—[c]	0.0010	0.0018	0.43 ± 0.04
(II) 0.1 M $TBAClO_4$ (O)–20 mM TBACl (W)	–0.234	–69		0.0020	0.0025	0.0030		1.26 ± 0.07
(III) 0.25 M $TBAClO_4$ (O)–10 mM TBACl (W)	–0.192	–65	0.0013	0.0018	0.0025			1.25 ± 0.05
(IV) 0.25 M $TBAClO_4$ (O)–10 mM $NaClO_4$ (W)	–0.165	–62	0.0020	0.0035	0.0045			2.19 ± 0.17
(V) 0.1 M $TBAClO_4$ (O)–20 mM $NaClO_4$ (W)	–0.123	–58	0.0027	0.0035	0.0050	0.0065		2.53 ± 0.16
(VI) 50 mM $TBAClO_4$ (O)–50 mM $NaClO_4$ (W)	–0.082	–54		0.0025	0.0040	0.0045		1.82 ± 0.17
CdTPP								
(VII) 0.1 M $TBAClO_4$ (O)–20 mM $NaClO_4$ (W)	–0.123	–40		0.0030				(2.0)[d]

[a] Estimated from Eq. (3) with the reported values of $\Delta_O^W\phi_X^\circ$ [47–49].

[b] Calculated by Eq. (8) with $E_W^{\circ'} - E_O^{\circ'} = -0.48$ V (for ZnTPP) or –0.29 V (for CdTPP).

[c] The value was too small to determine.

[d] Probably owing to the relative instability of CdTPP, the measurement was successful only in a single concentration condition.

Table 3

Kinetic parameters obtained with Cells A and B

Organic solvent	η[a] (10^{-3} Pa s)	λ[b] (kJ mol^{-1})	κZ_{het}[c] (cm s^{-1})	k_D[d] (cm M^{-1} s^{-1})	k_{uni}[e] (cm s^{-1})
Cell A					
DCE	0.779	83.4	3.6×10^{-4}	6.0 (137)[f]	3.1×10^{-6}
NB	1.795	82.3	9.0×10^{-4}	5.2 (61)[f]	2.7×10^{-6}
DCH	2.04	79.9	1.9×10^{-3}	5.0 (53)[f]	2.6×10^{-6}
NPOE	13.8	82.7	2.1×10^{-3}	2.6 (10)[f]	1.3×10^{-6}
Cell B					
NB	1.795	43	4.0×10^{-6}	3.0 (40)[f]	9.7×10^{-7}

[a] Viscosity of the organic solvent; the values are taken from Ref. [52] or [45] (for DCH).

[b] Estimated theoretically for Cell A and obtained as an adjusting parameter for Cell B.

[c,d] Obtained by curve fitting.

[e] Calculated by Eq. (11).

[f] Values in parentheses are the k_D values estimated theoretically by Eq. (2) with $D_A = 8.6 \times 10^{-6}$, 3.8×10^{-6}, 3.3×10^{-6}, 6.4×10^{-7} cm^2 s^{-1} for DcMFc in DCE, NB, DCH, and NPOE, respectively, and with $D_A = 1.9 \times 10^{-6}$ cm^2 s^{-1} for $MTPP^+$ in NB.

Figure captions

Fig. 1. Previous model for the formulation of a diffusion-controlled rate constant of ET at an O/W interface [39].

Fig. 2. Cells A and B used in the SECM measurements, respectively, for (A) the DcMFc–$Fe(CN)_6^{3-}$ system and for (B) the $MTPP^+$–$Fe(CN)_6^{4-}$ system. In Cell A, (1) *x* M DcMFc, 10–50 mM TAATPB; (2) 1 mM $K_4Fe(CN)_6$, 10–50 mM TAACl, 0.5 M NaCl; (3) 3.0 M NaCl. In Cell B, (4) 0.5 mM MTPP (M = Zn, Cd), 0.05–0.25 M $TAAClO_4$; (5) *y* M $K_4Fe(CN)_6$, 0.5 M NaCl; (6) 10–20 mM TBACl or $NaClO_4$; (7) 3.0 M NaCl. Phases 6 and 7 were separated by using a hollow gel pellet [24]. (WE) working electrode, (RE) reference electrode, (CE) counter electrode.

Fig. 3. Approach curves obtained (A) with Cell A for different concentrations of DcMFc and (B) with Cell B (with ZnTPP) for different concentrations of $Fe(CN)_6^{4-}$. In both cells, the O-phase solvent was NB. Electrolyte conditions: (A) 20 mM TEATPB (O)–20 mM TEACl (W); (B) 0.1 M $TBAClO_4$ (O)–20 mM $NaClO_4$ (W). Open circles: experimental values in the presence of the indicated concentrations of DcMFc or $Fe(CN)_6^{4-}$. Solid lines: theoretical curves for the corresponding concentrations and the blank. The dashed lines represent the diffusion-limited curves.

Fig. 4. Dependence of k_f on the concentrations of (A) DcMFc and (B) $Fe(CN)_6^{4-}$ in Cell A and Cell B (with ZnTPP), respectively. The plots in panel (A) correspond to the electrolyte conditions of (○) I, (△) II, (□) III, (×) IV, (◇) V, and (∗) VI shown in Table 1, whereas those in panel (B) correspond to the electrolyte conditions of (○) I, (△) II, (□) III, (×) IV, (◇) V, and (∗) VI shown in Table 2.

Fig. 5. Driving force dependence of the second-order rate constant for the ET between

DcMFc in NB and $Fe(CN)_6^{3-}$ in W. Solid line: the theoretical curve obtained by curve fitting.

Fig. 6. Driving force dependence of the second-order rate constant for the ET between (●) $ZnTPP^+$ or (▲) $CdTPP^+$ in NB and $Fe(CN)_6^{4-}$ in W. The plot for $CdTPP^+$, shown in parentheses, was obtained under a single concentration condition. The plot for $CdTPP^+$ (△) is based on the data previously obtained by *ac* impedance method [8]. Solid line: the fitting curve obtained with three adjusting parameters (k_D, κZ_{het}, and λ; see Table 3). Dashed line: the fitting curve obtained with the theoretical value of k_D (= 40 cm M^{-1} s^{-1}) and two adjusting parameters ($\kappa Z_{het} = 1.5 \times 10^{-6}$ cm s^{-1} and $\lambda = 43$ kJ mol^{-1}).

Fig. 7. Two possible models for understanding the bimolecular reaction effect of ET at the O/W interface, which are based on (a) "microscopic diffusion" and (b) "interfacial diffusion".

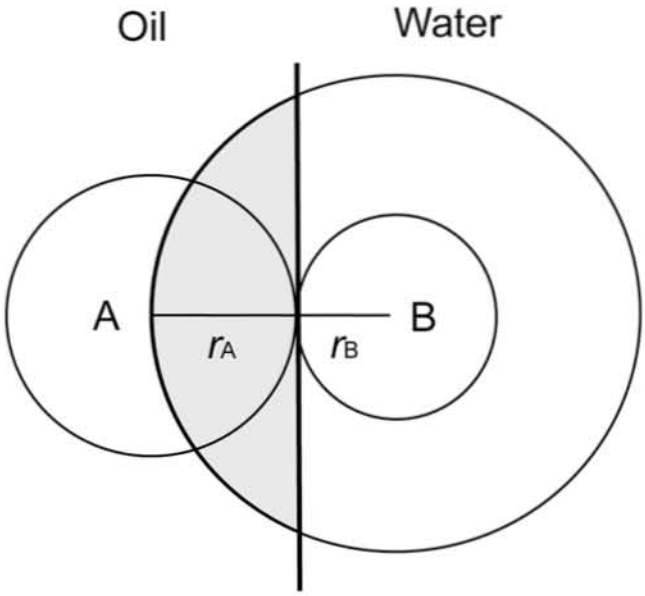

Fig. 1

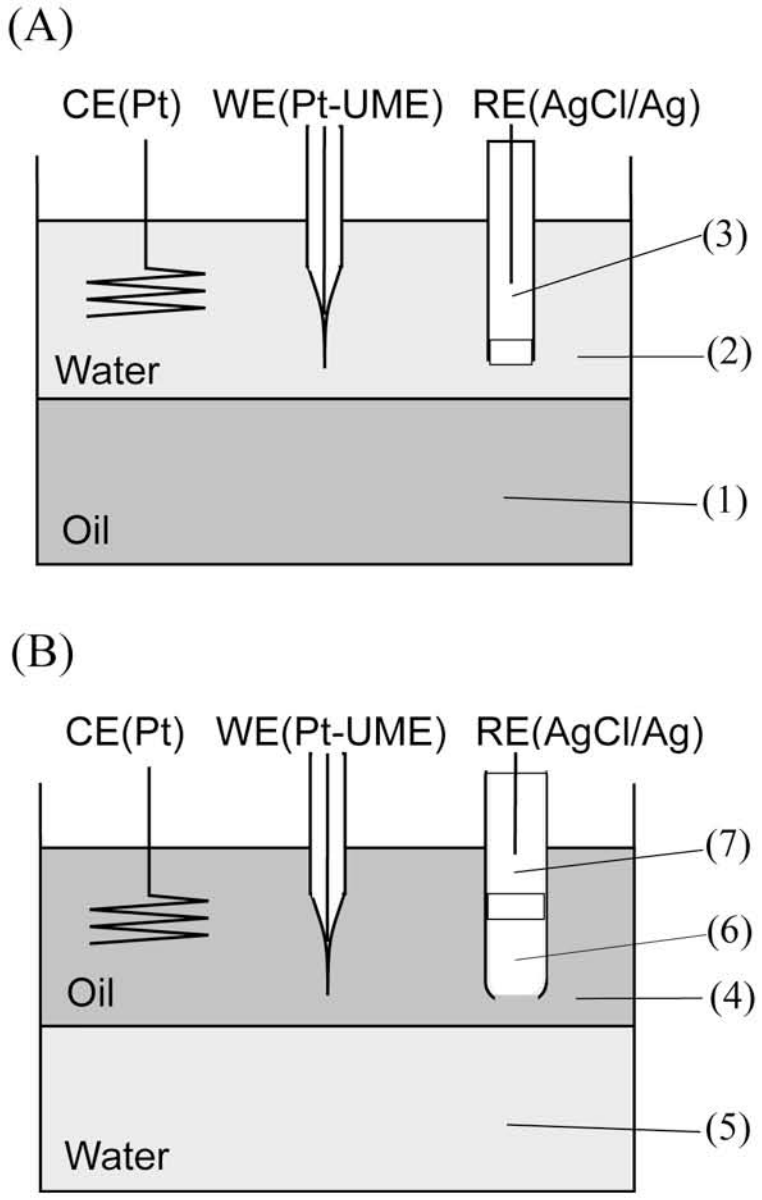
(A)
CE(Pt)
WE(Pt-UME)
RE(AgCl/Ag)
(3)
(2)
Water
(1)
Oil
(B)
CE(Pt)
WE(Pt-UME)
RE(AgCl/Ag)
(7)
(6)
Oil
(4)
(5)
Water

Fig. 2

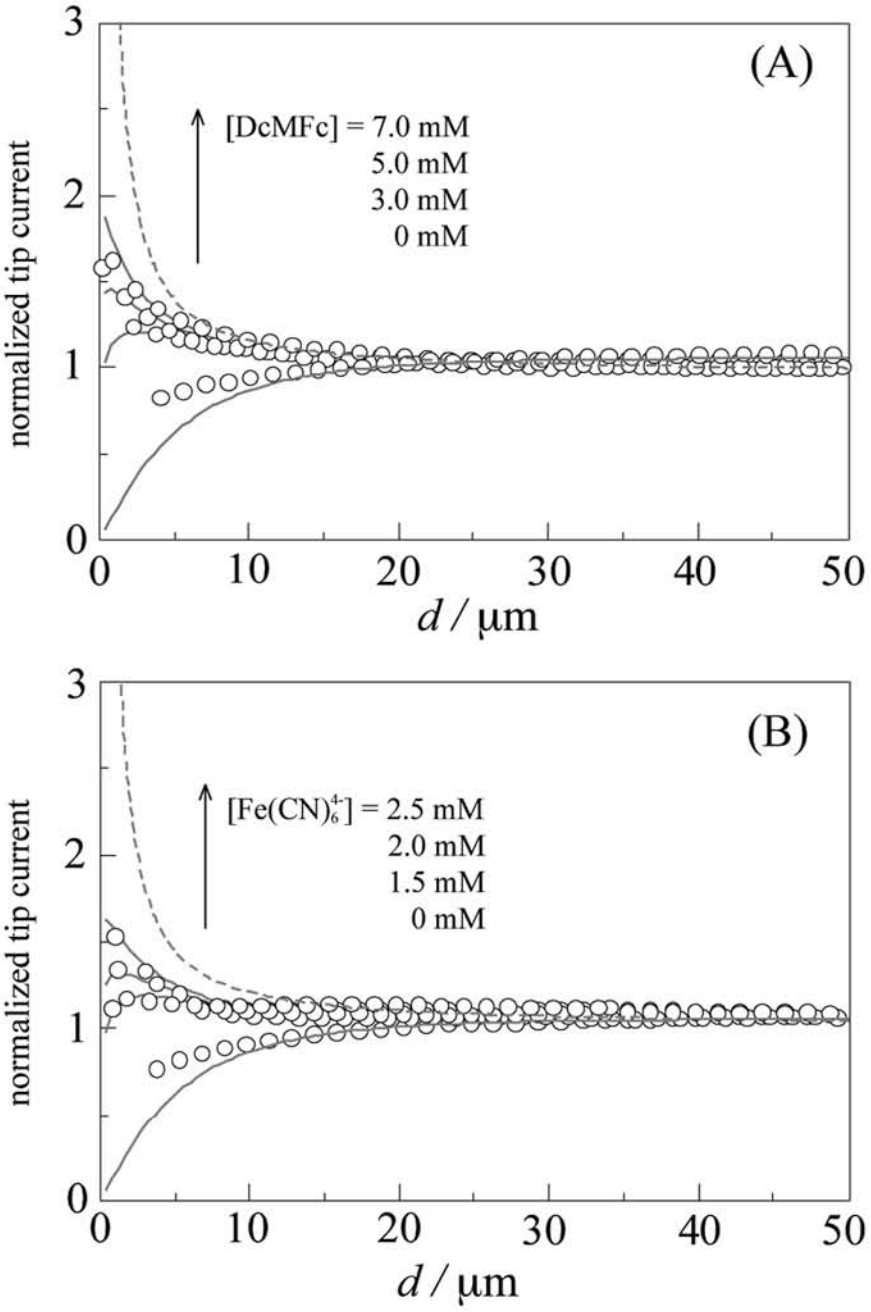
(A)
[DcMFc] = 7.0 mM
5.0 mM
3.0 mM
0 mM
normalized tip current
d / μm
(B)
[Fe(CN)6 4-] = 2.5 mM
2.0 mM
1.5 mM
0 mM
normalized tip current
d / μm

Fig. 3

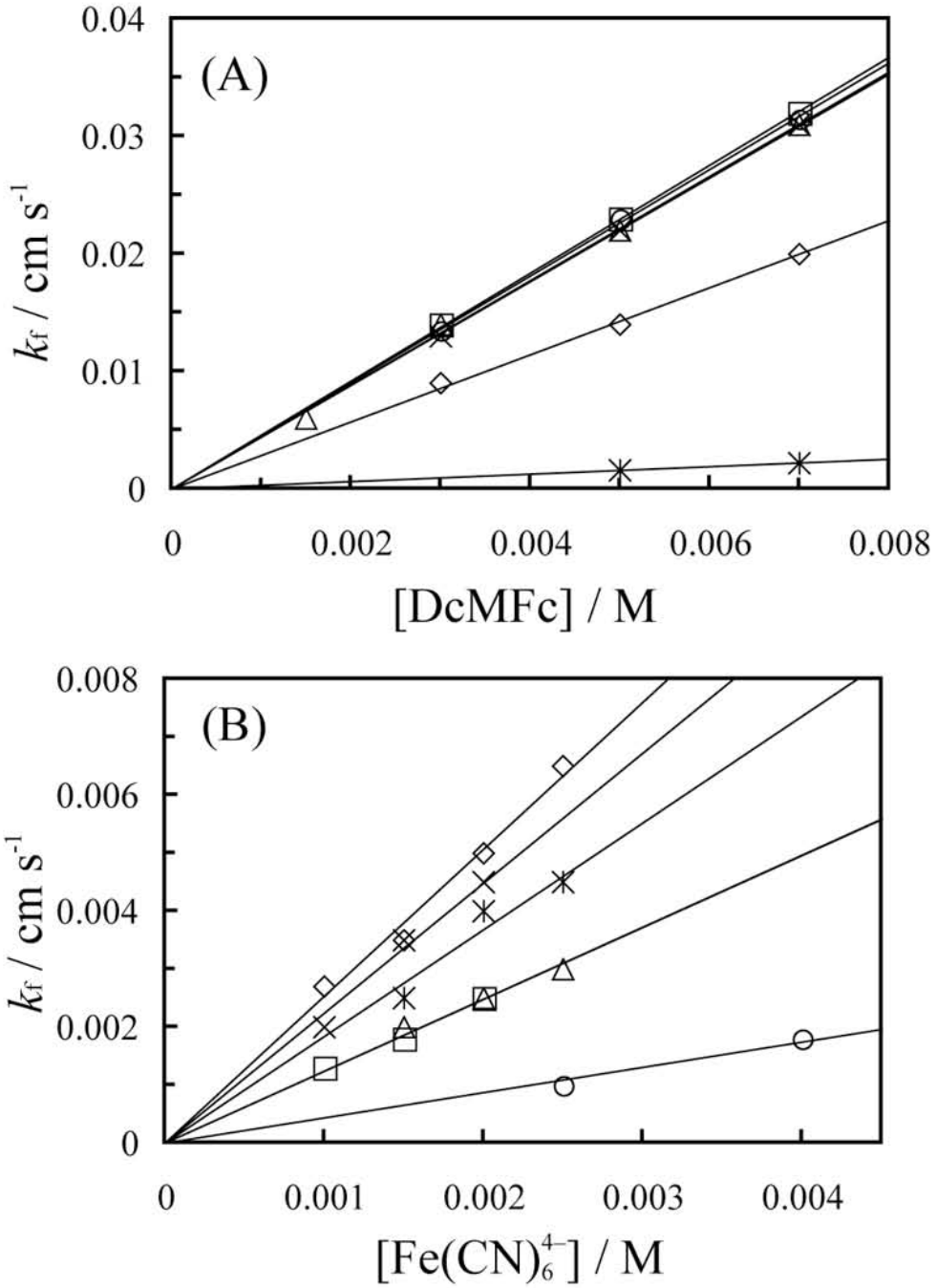
(A)
0.04
0.03
0.02
0.01
0
k_f / cm s^{-1}
0
0.002
0.004
0.006
0.008
[DcMFc] / M
(B)
0.008
0.006
0.004
0.002
0
k_f / cm s^{-1}
0
0.001
0.002
0.003
0.004
[Fe(CN)$_6^{4-}$] / M

Fig. 4

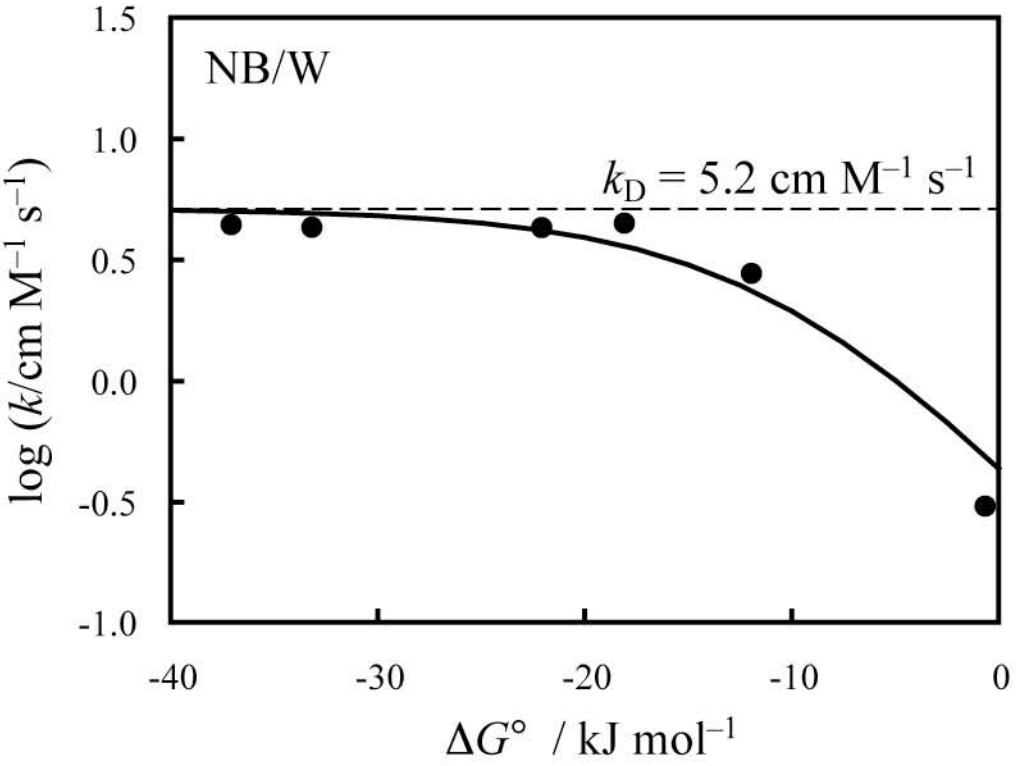
NB/W
k_D = 5.2 cm M^{-1} s^{-1}
log (k/cm M^{-1} s^{-1})
1.5
1.0
0.5
0.0
-0.5
-1.0
-40
-30
-20
-10
0
$\Delta G°$ / kJ mol^{-1}

Fig. 5

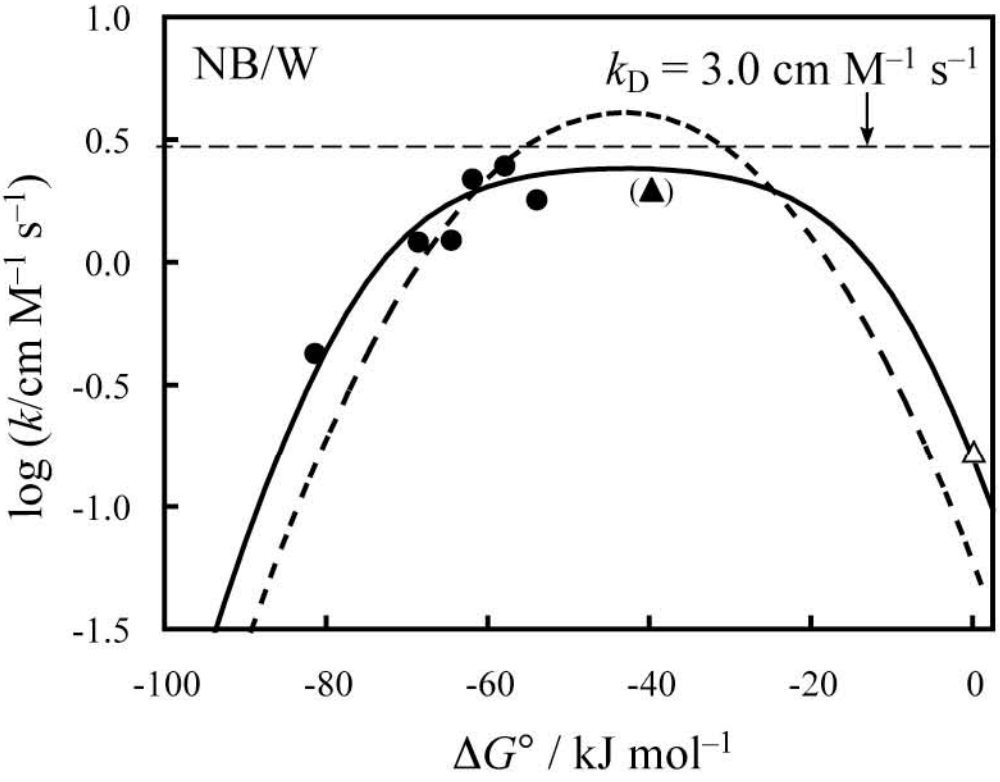
NB/W
k_D = 3.0 cm M^{-1} s^{-1}
log (k/cm M^{-1} s^{-1})
1.0
0.5
0.0
-0.5
-1.0
-1.5
-100
-80
-60
-40
-20
0
$\Delta G°$ / kJ mol^{-1}

Fig. 6

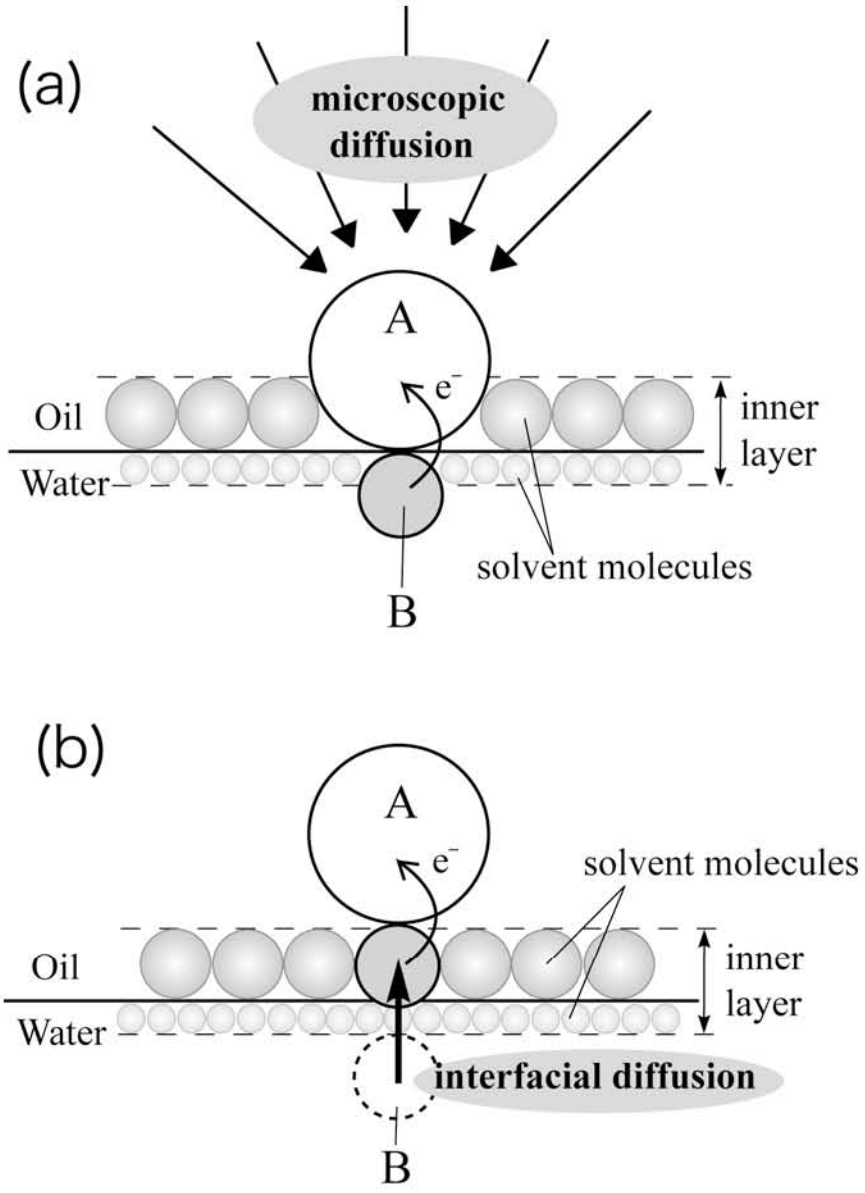
(a)
microscopic diffusion
A
e⁻
Oil
Water
inner layer
solvent molecules
B
(b)
A
e⁻
solvent molecules
Oil
Water
inner layer
interfacial diffusion
B

Fig. 7

Supplementary material

Bimolecular-reaction effect on the rate constant of electron transfer at the oil/water interface as studied by scanning electrochemical microscopy

Toshiyuki Osakai,* Masanori Okamoto, Takayasu Sugihara, Kiyoharu Nakatani

Table S1

Kinetic data obtained with Cell A for the DCE/W interface

Electrolyte conditions	$\Delta_O^W\phi$ [a] (V)	$\Delta G°$ [b] (kJ mol^{-1})	k_f (cm s^{-1}) [DcMFc] (M) 0.002	0.003	0.005	0.007	$k \pm$ SD (cm M^{-1} s^{-1})
(I) 20 mM TEATPB (O)–20 mM TEACl (W)	0.020	–35	0.0100	0.0130	0.0250		4.78 ± 0.38
(II) 10 mM TEATPB (O)–50 mM TEACl (W)	–0.021	–31	0.0100	0.0135	0.0230		4.70 ± 0.26
(III) 20 mM TPrATPB (O)–20 mM TPrACl (W)	–0.090	–24	0.0075	0.0110	0.0190		3.74 ± 0.07
(IV) 20 mM TBATPB (O)–20 mM TBACl (W)	–0.220	–12		0.0045	0.0070	0.0110	1.49 ± 0.09

[a] Estimated from Eq. (3) with the reported values of $\Delta_O^W\phi_X^\circ$ [47,50].

[b] Calculated by Eq. (8) with $E_W^{\circ'} - E_O^{\circ'} = 0.34$ V.

Table S2

Kinetic data obtained with Cell A for the DCH/W interface

Electrolyte conditions	$\Delta_O^W\phi$ [a] (V)	$\Delta G°$ [b] (kJ mol^{-1})	k_f (cm s^{-1}) [DcMFc] (M) 0.002	0.003	0.005	0.007	$k \pm$ SD (cm M^{-1} s^{-1})
(I) 20 mM TEATPB (O)–20 mM TEACl (W)	0.056	–35		0.0160	0.0200	0.0340	4.73 ± 0.68
(II) 10 mM TEATPB (O)–50 mM TEACl (W)	0.015	–31	0.0095	0.0130		0.0300	4.46 ± 0.26
(III) 20 mM TPrATPB (O)–20 mM TPrACl (W)	–0.072	–23		0.0130	0.0220	0.0300	4.34 ± 0.06
(IV) 20 mM TBATPB (O)–20 mM TBACl (W)	–0.220	–9		0.0080	0.0130	0.0180	2.61 ± 0.05
(V) 20 mM TPnATPB (O)–20 mM TPnACl (W)	–0.343	3		0.0025	0.0040	0.0056	0.81 ± 0.02

[a] Estimated from Eq. (3) by regarding the midpoint potentials in CV [45] as $\Delta_O^W\phi_X^\circ$.

[b] Calculated by Eq. (8) with $E_W^{\circ'} - E_O^{\circ'} = 0.31$ V.

Table S3

Kinetic data obtained with Cell A for the NPOE/W interface

Electrolyte conditions	$\Delta_O^W\phi$ [a] (V)	$\Delta G°$ [b] (kJ mol^{-1})	k_f (cm s^{-1}) [DcMFc] (M) 0.003	0.005	0.007	$k \pm$ SD (cm M^{-1} s^{-1})
(I) 20 mM TEATPB (O)–20 mM TEACl (W)	0.026	–37	0.0085	0.0130	0.0170	2.62 ± 0.20
(II) 10 mM TEATPB (O)–50 mM TEACl (W)	–0.015	–33	0.0075	0.0120	0.0170	2.44 ± 0.05
(III) 20 mM TPrATPB (O)–20 mM TPrACl (W)	–0.092	–26	0.0090	0.0130	0.0170	2.68 ± 0.29
(IV) 20 mM TBATPB (O)–20 mM TBACl (W)	–0.241	–12	0.0075	0.0100	0.0140	2.17 ± 0.29
(V) 20 mM TPnATPB (O)–20 mM TPnACl (W)	–0.324	–3	0.0035	0.0060	0.0080	1.17 ± 0.03

[a] Estimated from Eq. (3) with the reported values of $\Delta_O^W\phi_X^\circ$ [47,51,52].

[b] Calculated by Eq. (8) with $E_W^{\circ'} - E_O^{\circ'} = 0.36$ V.

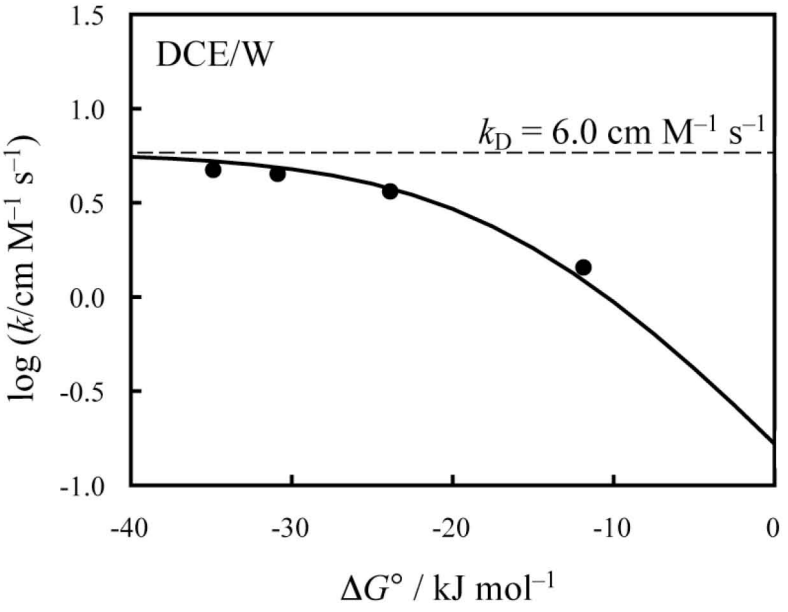

Fig. S1. Driving force dependence of the second-order rate constant for the ET between DcMFc in DCE and $Fe(CN)_6^{3-}$ in W. Solid line: the theoretical curve obtained by curve fitting.

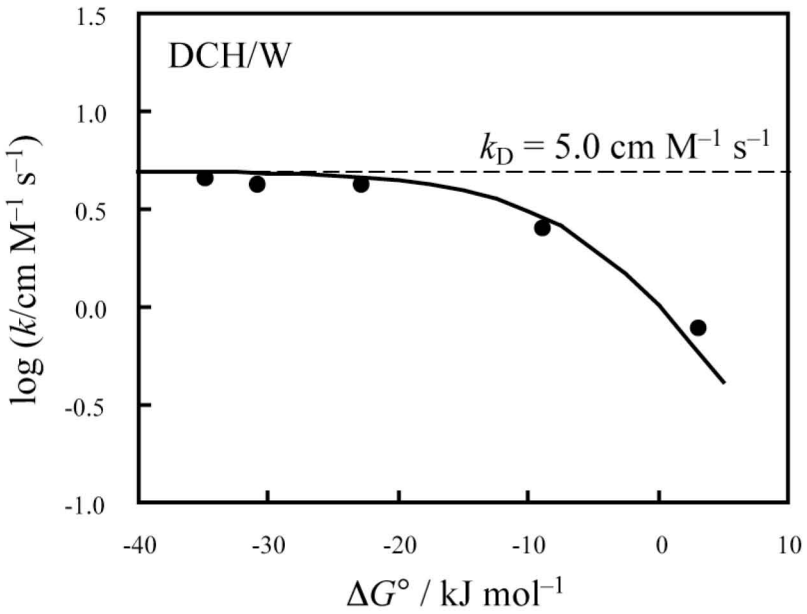

Fig. S2. Driving force dependence of the second-order rate constant for the ET between DcMFc in DCH and $Fe(CN)_6^{3-}$ in W. Solid line: the theoretical curve obtained by curve fitting.

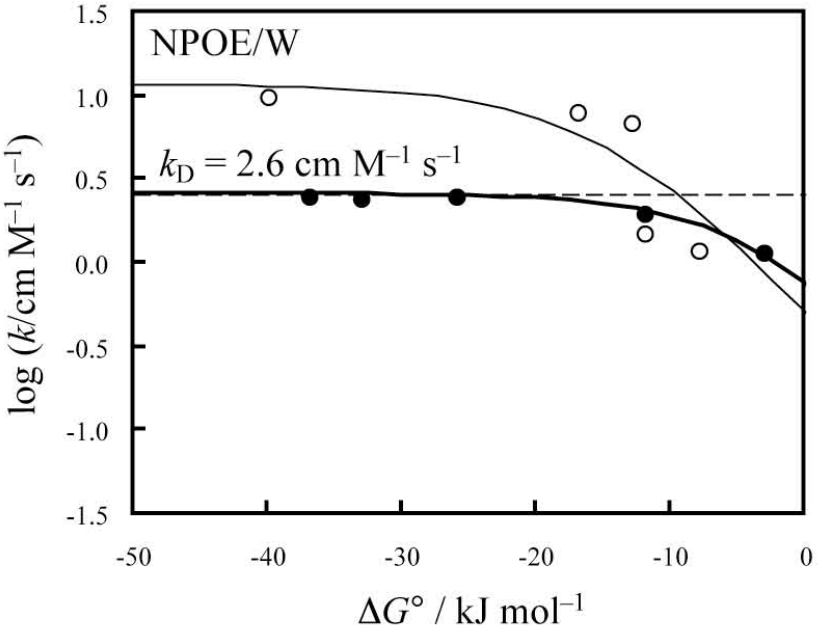

Fig. S3. Driving force dependence of the second-order rate constant for the ET between DcMFc in NPOE and $Fe(CN)_6^{3-}$ in W, which were observed by (●) SECM and (○) CV with a single micro W-droplet [27]. Thick and thin solid lines: the corresponding theoretical curves obtained by curve fitting. For the later curve, the following parameters were used: $\kappa Z_{het} = 1 \times 10^{-2}$ cm s^{-1}, λ = 108 kJ mol^{-1}, k_D = 12 cm M^{-1} s^{-1}, and $k_{uni} = 4.76 \times 10^{-6}$ cm s^{-1}.